Cite this: DOI: 10.1039/c0xx00000x

www.rsc.org/xxxxxx

Full Paper

Electro-oxidation of hydrazine at gold nanoparticle functionalised single walled carbon nanotube network ultramicroelectrodes

Petr V. Dudin, Patrick R. Unwin* and Julie V. Macpherson*

Received (in XXX, XXX) Xth XXXXXXXXX 20XX, Accepted Xth XXXXXXXXX 20XX

DOI: 10.1039/b000000x

Networks of pristine single walled carbon nanotubes (SWNTs) grown by catalysed chemical vapour deposition (cCVD) on an insulating surface and arranged in an ultramicroelectrode (UME) format are insensitive to the electro-oxidation of hydrazine (HZ) in aqueous solution, indicating a negligible metallic nanoparticle content. Sensitisation of the network towards HZ oxidation is promoted by the deliberate and controlled electrodeposition of "naked" gold (Au) nanoparticles (NPs). By controlling the deposition conditions (potential, time) it is possible to control the size and spacing of the Au NPs on the underlying SWNT network. Two different cases are considered: Au NPs at a number density of 250 ± 13 NPs μm^{-2} and height 24 nm ± 5 (effective surface coverage, θ, = 92%) and (ii) Au NPs of number density ~ 22 ± 3 NPs μm^{-2} and height 43 nm ± 8 nm (θ = 35%). For both morphologies the HZ oxidation half-wave potential ($E_{1/2}$) is shifted significantly negative by ca. 200 mV, compared to a gold disc UME of the same geometric area, indicating significantly more facile electron transfer kinetics. $E_{1/2}$ for HZ oxidation for the higher density Au NP-SWNT structure is shifted slightly more negative (by ~ 25 mV) than $E_{1/2}$ for the lower density Au NP electrode. This is attributed to the lower flux of HZ at NPs in the higher number density arrangement (smaller kinetic demand). Importantly, using this approach, the calculated HZ oxidation current density sensitivities for the Au NP – SWNT electrodes reported here are higher than for many other metal NP functionalised carbon nanotube electrodes.

Introduction

The combination of metal nanoparticles (NPs) with conducting support surfaces has proven powerful for the electrocatalytic detection of many chemical species.[1, 2] A particularly interesting support platform, which has attracted much interest, is the carbon nanotube (CNT), which offers interesting intrinsic physical properties, such as excellent electrical conductivity,[3] low intrinsic capacitance in the pristine state,[4] and ease of functionalisation with a variety of materials, including NPs.[5] There are two common approaches to producing NP-CNT composite electrodes. The first involves the pre-synthesis of the NPs by chemical means, resulting in ligand-stabilised NPs which are then dispersed onto the CNT matrix.[6] The second uses electrodeposition procedures to directly nucleate and grow "naked" NPs on the CNT. Advantages of the latter method are that NPs are likely to be more active and there is the possibility of controlling the size and spacing of the NPs on the CNTs by simply adjusting the applied potential and deposition time.[7-10]

Recent work on the electrochemical characteristics of CNTs has considered the quality of the CNT on the electrochemical response.[5] Notably, many of the popular growth techniques for CNT production, such as arc discharge and HiPCO used by many of the commercial suppliers of CNTs, result in CNTs with a high metallic (e.g. Co, Fe, Mo) content. Even after stringent acid washing procedures it has been shown that the metal content cannot be completely removed.[5, 11] Hence, an emerging view is that many electrocatalytic processes observed on functionalised CNT electrodes are due to residual catalytic NPs remaining from the growth process.[12-14]

The considerable attributes of pristine CNTs (particularly single walled carbon nanotubes, SWNTs) arranged randomly in a conductive network on insulating substrates, produced by catalysed chemical vapour deposition (cCVD), for electroanalysis, have been demonstrated.[15-18] Notably, the SWNT networks on Si/SiO_2 show an electrochemical response resulting solely from the CNTs, very low background currents (due to the low surface coverage and low capacitance of pristine SWNTs)[7, 17] and fast response times.[16]

The focus of this paper is the detection of hydrazine (HZ). HZ is a carcinogenic, toxic, electroactive compound with numerous industrial applications, such as in drug synthesis, explosives, plating, corrosion protection and as a rocket fuel.[19] HZ has also been considered as a "zero emission" fuel for fuel cells.[20] The development of strategies which enable its detection is thus incredibly important, with electrochemical detection representing a promising route forward. Metals such as platinum, palladium, rhodium, gold, iron, cobalt, molybdenum and metal-conductive polymer composites have all previously been shown to be

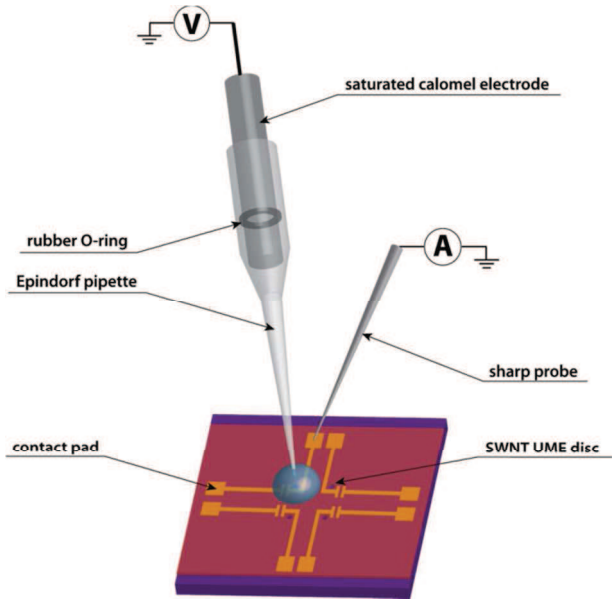

Figure 1. Schematic of the two-electrode setup employed in the HZ oxidation experiments. A saturated calomel electrode (SCE) was mounted inside a pipette tip and held in place using an O-ring. A 15 µL drop of electrolyte solution was placed on top of a SWNT network UME defined by photolithography

capable of electrocatalysing HZ oxidation.[12, 21, 22]

In this paper we demonstrate an electrochemical platform for HZ detection based on networks of high purity, pristine SWNTs, which importantly, contain negligible amounts of catalytically active metal NPs. We then *deliberately* impart electrocatalytic activity to the underlying SWNT structure in a controlled manner through the use of metal electrodeposition techniques. By using an insulating support substrate, nucleation takes place only on the SWNTs, without complication from the underlying surface. We deploy the SWNT network in an ultramicroelectrode (UME) format, in which the SWNTs provide a 1D support structure for NP formation and the 2D UME arrangement offers excellent electrical conductivity and extremely low background currents. We focus on Au NPs as the electrocatalytic surface, as we have recently elucidated the mechanism of Au electrodeposition on SWNT networks,[7] allowing control of the electrodeposited nanostructures. We show how by changing the deposition morphology it is possible to influence HZ electro-oxidation.

Experimental

SWNT Growth and Characterisation

SWNTs were grown on 1.8 mm × 1.8 mm Si/SiO_2 chips (IDB Technologies Ltd., 300 nm of thermally grown oxide) by cCVD using a sub-monolayer coverage of Co as a catalyst (Quorum Technologies SC7640 sputter coater at 0.5 kV for 10 s). The use of cCVD enables the growth of SWNTs on insulating surfaces, without the need for further purification, due to a significantly reduced amorphous carbon and metal content.[15] The substrates were heated to 850 °C for 20 minutes under a H_2 flow of 150 standard cubic centimetres per minute (sccm). A bubbler, through which Ar was flowed at 850 sccm, was employed to deliver ethanol vapour (carbon source for SWNT growth) into the cCVD growth chamber. SWNT growth was continued for 10 min; the Ar flow was then switched off and the system was left to cool under just a flow of H_2.

High Resolution Microscopy

Atomic Force Microscopy (AFM) images were acquired in tapping mode using a Bruker Nano Enviroscope AFM (with a Nanoscope IV controller). SPIP software (Image Metrology) was employed for analysis of the Au NP heights. For each deposition surface, three AFM images were recorded, in random locations, from which statistical information on Au NP heights was obtained. Field emission - scanning electron microscopy (FE-SEM) images were taken using a SUPRA 55 variable pressure system (Zeiss) at 10 kV to visualise the Au NPs and CNTs. Again, three FE-SEM images were acquired, in random locations, from which statistical information on Au NP surface coverage was obtained. Micro-Raman (Renishaw in Via Microscope coupled to a Leica microscope) was used to record Raman spectra, using an Ar laser at excitation wavelength 514.5 nm (2.41 eV at 10 mW power) focused in a 2.5 µm diameter spot with 50 s exposure time.

UME Disc Device Fabrication

The procedure for SWNT UME device fabrication (here ~ 100 µm diameter discs) was described in detail elsewhere.[16] Briefly, fabrication involved gold contact evaporation through a shadow mask (70 nm of Au with 2 nm Cr adhesive layer) followed by coating with a photoresist (S1818) from which UME discs were defined using a mask aligner (MJB4, Süss MicroTec) with 4.5 s exposure time. The same procedure was employed for fabrication of the evaporated gold (Au_{evap}) UMEs except the discs were defined in the region of the gold contact. Prior to use the Au_{evap} UMEs were cycled in 0.1 M phosphate buffer solution (PBS), at potentials sufficient to form and strip gold oxide from the surface, until a reproducible response was obtained.

Solutions

All solutions were made with Milli-Q reagent water (Millipore Corp., 18.2 MΩ cm at 25 °C). Gold electrodeposition solutions consisted of 1 mM $KAuCl_4$ (99.999%, Aldrich) in 0.2 M $NaClO_4$. Hydrazine sulphate (99%, Aldrich) (30% solution in water, Fluka) was prepared in 0.1 M PBS at pH 7.2 (Aldrich). Aqueous solutions of redox-active (trimethylammonium) methylferrocene(+) ($FcTMA^+$) contained 0.2 M $NaClO_4$ (Fisher Scientific) as a supporting electrolyte. $FcTMA^+$ hexafluorophosphate was prepared via metathesis of the corresponding iodide salt (99%, Strem) with ammonium hexafluophosphate (99.5%, Strem).

Electrochemical setup and experiment

All potential step chronoamperometry (CA) and cyclic voltammetry (CV) experiments were performed in a droplet cell, using a two-electrode arrangement. A drop of the electrolyte solution was placed over the UME and the drop was contacted by a reference electrode. Given the small volume of the droplet (15 µL) a conventional saturated calomel electrode (SCE) was placed

inside an Epindorf pipette tip, which dipped into the

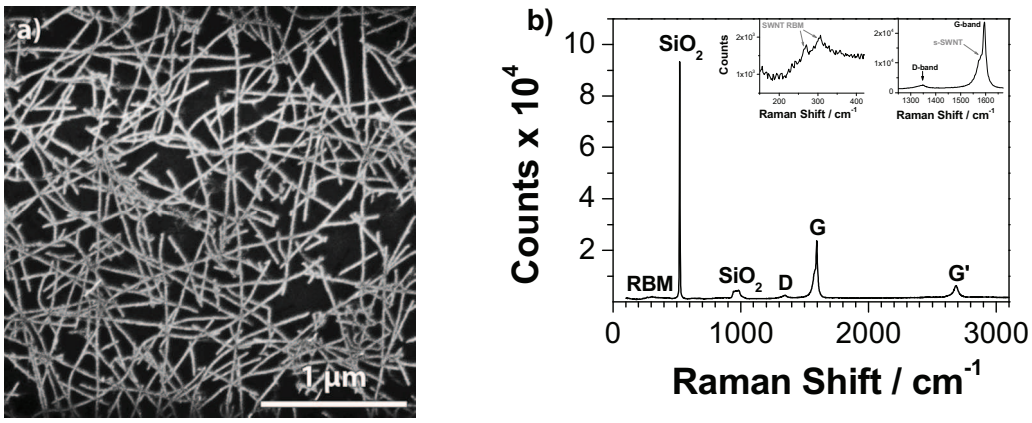

Figure 2. (a) FE-SEM image of a typical SWNT network employed in the study. Note due to charging effects the SWNTs appear wider than they actually are. (b) Micro-Raman spectrum of the SWNT network. Inset shows magnified parts of the spectrum showing in more detail (left) radial breathing modes (RBM) and (right) D and G peaks.

droplet and was filled with the analyte. An O-ring was placed on the SCE glass body in order to prevent electrolyte leakage from the pipette tip. A schematic of the experimental set-up is shown in Figure 1. The CNT network, which functioned as the working electrode, was contacted by a 100 nm thick evaporated Au band (2 nm Cr underlayer) which did not come into contact with the solution. Electrical connection to the Au contact was made with a sharp tip probe (*xyz* 300TR Quater Research). All the potentials reported in the work are quoted with respect to SCE. All measurements were made with a CH Instruments Model 600B potentiostat (Austin, TX).

Functionalisation of the SWNT UMEs with Au NPs was achieved by electrochemical deposition from a solution containing 1 mM $KAuCl_4$ in 0.2 M $NaClO_4$, using CA, by stepping the potential from +750 mV (where neither reduction nor oxidation of $AuCl_4^-$ occurs) to a defined deposition potential for a given period of time (*vide infra*).

Results and discussions

Figure 2(a) shows a representative FE-SEM image of SWNTs produced by cCVD growth. The SWNT structure is clearly two-dimensional with a single layer of SWNTs arranged in a network on the insulating Si/SiO_2 support at a density of >8 µm length of SWNT per μm^2 (μm_{SWNT} μm^{-2}) as measured from FE-SEM images. A typical micro-Raman spectrum of the sample covering the 1300-1700 cm^{-1} region, where both the tangential modes derived from the in-plane Raman vibrations in graphite (G-band, 1550-1600 cm^{-1}) and the disorder modes (D-band, 1300-1400 cm^{-1}) are visible, is shown in Figure 2(b). The shape and position of the G-band confirms the presence of semiconducting (G-band shoulder) and metallic SWNTs and the very small D-band intensity indicates they are of high quality, i.e. there is minimal amorphous carbon (Figure 2 (b) inset). Distinct radial breathing mode (RBM) peaks (Figure 2 (b) inset) also indicate that the sample contains a significant amount of SWNTs, with calculated diameters in the range 1.2 - 1.5 nm.[23] The SWNT nature of the network was further confirmed by AFM image analysis which revealed SWNTs with heights typically of 1-3 nm. In some cases slightly larger SWNTs were observed which could either indicate SWNT bundles, or, perhaps, small multi-walled or double-walled nanotubes.

In order to ascertain whether the as-grown SWNT network could promote the electro-oxidation HZ, CVs were recorded at a scan rate of 100 mV s^{-1} at a 100 µm diameter SWNT network disc UME in 5 mM HZ solution in 0.1 M PBS (pH 7.2), Figure 3(a). In the potential range +0.8 V to -0.8 V (versus SCE) there is no discernible faradaic response, signifying that HZ is electro-inactive at the SWNT network. There is also no evidence of a current signal due to the reduction of oxygen, in this potential window. Based on recent studies which have determined that residual catalyst impurities such as Fe, Co and Mo are responsible for the electrocatalytic oxidation of hydrazine

Cite this: DOI: 10.1039/c0xx00000x

www.rsc.org/xxxxxx

Full Paper

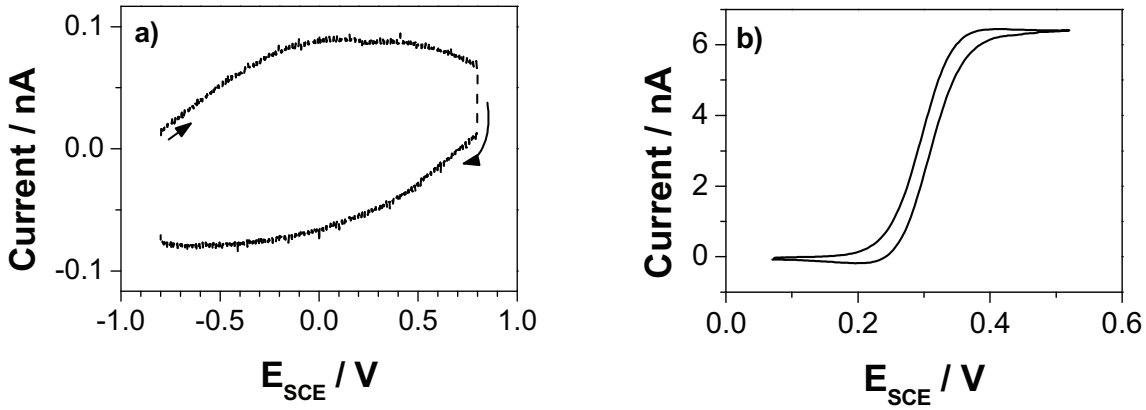

Figure 3. CVs recorded at the same 100 µm diameter SWNT network UME in a solution containing (a) 5 mM hydrazine in 0.1 M PBS (pH 7.2) at a scan rate of 100 mV s^{-1} and (b) 0.5 mM $FcTMA^+$ oxidation (in 0.2 M $NaClO_4$) at a scan rate of 4 mV s^{-1}. Note the difference in current scales.

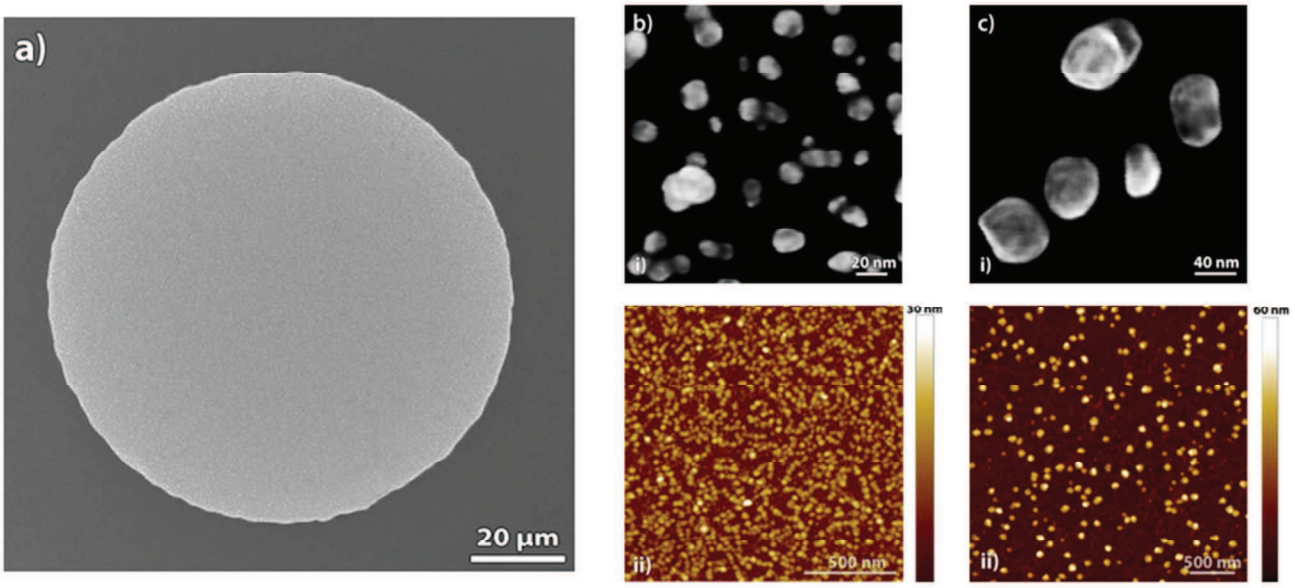

Figure 4. FE-SEM image of (a) a 100 µm diameter disk SWNT network UME decorated with Au NPs electrodeposited from a solution containing 1 mM $KAuCl_4$ and 0.2 M $NaClO_4$, at +550 mV for 15s. Representative higher resolution FE-SEM (i) and AFM (ii) images of AuNP-SWNT electrodes formed by electrodeposition at (b) -800 mV versus SCE, for 12 s and (c) +550 mV for 15 s.

at CNTs,[11, 12] these results, complemented by the Raman and microscopy data (Figure 2), indicate that the cCVD SWNTs, contain negligible quantities of electrocatalytically active Co NPs. Thus, further processing of the SWNTs to remove contaminants is not required. This is an important attribute of this material as SWNTs which have been stringently acid cleaned prior to two-dimensional network formation would be much shorter resulting in, for the same geometric area, a significantly increased number of SWNT-SWNT contacts, which results in an increased electrical resistance of the material.

Of interest is why the SWNT itself is not catalytically electroactive for HZ oxidation. Fundamental studies on single crystal Pt, Rh and Au surfaces have shown that adsorption of HZ

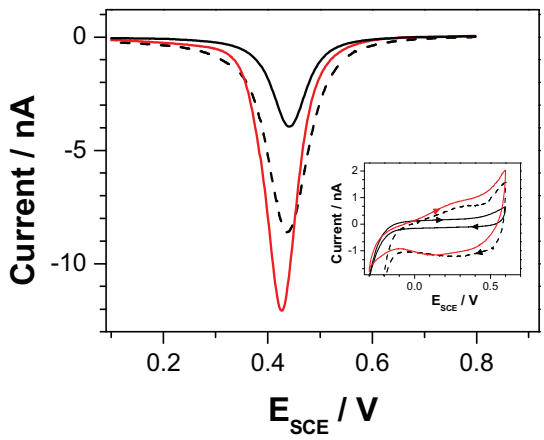

Figure 5. Linear sweep voltammetry for the reduction of deposited gold oxide, recorded at a scan rate of 20 mV s^{-1}, after an oxidation potential of +1.2 V was applied to the electrode for 20 s to form the surface oxide in 0.1 M PBS (pH 7.2) on (i) Au NP-SWNT electrode deposited at -800 mV for 12s (dashed black line); (ii) Au NP-SWNT electrode deposited at +550 mV for 15s (solid black line) and (iii) Au_{evap} electrode (red line). The inset shows background CVs recorded in 0.1 M PBS at the three electrodes at a scan rate of 100 mV s^{-1}.

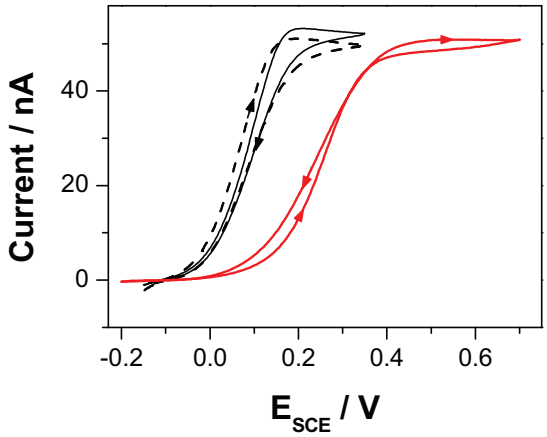

Figure 6. CVs for the oxidation of 0.5 mM HZ in 0.1 M PBS at a 100 µm diameter disk UME recorded at a scan rate of 10 mV s^{-1} at three different electrodes: (i) AuNP-SWNT electrode deposited at -800 mV for 12s (dashed black line); (ii) AuNP-SWNTs deposited at +550 mV for 15s (solid black line) and (iii) Au_{evap} electrode (red line).

and/or intermediates formed in the oxidation process are key steps in the electro-oxidation process.[20] Although there have been no specific binding studies (theoretical and or/experimental) of HZ (N_2H_4) to SWNTs, there have been numerous studies on the interaction between the closely related molecule, ammonia (NH_3) and a SWNT.[24] In essence for SWNTs, binding between NH_3 and the SWNT is calculated to be extremely weak; in fact experimental observations at room temperature show no evidence of NH_3 adsorption.[24] Consequently, HZ adsorption is also unlikely given the similarity between HZ and NH_3.

To confirm that this same UME was fully functioning as an electrode (even though no signal for HZ oxidation was detectable) an outer sphere redox species, $FcTMA^+$, which readily undergoes electron transfer at SWNTs,[16,25] was chosen for CV analysis. Figure 3(b) show a typical CV for the oxidation of 0.5 mM $FcTMA^+$ in 0.2 M $NaClO_4$ at a scan speed of 4 mV s^{-1}. The limiting steady-state current observed, i_{ss}, = 0.65 nA, is in agreement with the predicted value of 0.66 nA:[26]

$$i_{ss} = 4nFDC_br \quad (1)$$

where n is the number of electrons transferred per redox event (n =1), F is the Faraday constant, r is the radius of the disc electrode (r = 50 µm) and C_b and D refer to the bulk concentration and diffusion coefficient, respectively (D = 6.7 × 10^{-6} cm^2 s^{-1} for $FcTMA^+$[27]).

To sensitise the SWNT network towards HZ oxidation, SWNT UME discs were functionalized with Au NPs by electrochemical deposition, as outlined in the experimental section. We sought to produce two significantly different Au NP coverages and morphologies, for comparison, as validated by FE-SEM and AFM. Figure 4(a) shows a typical low resolution FE-SEM image of an Au NP-decorated SWNT network UME after electrodeposition for 15 s at +550 mV. Higher resolution FE-SEM (i) and AFM (ii) images are also shown after electrodeposition at a potential of −800 mV for 12 s (Fig. 4(b)) and +550 mV for 15 s (Fig. 4(c)).

Electrodeposition at −800 mV for 12 s resulted in a high coverage of relatively small Au NPs, 250 ± 13 NPs $µm^{-2}$ (measured using FE-SEM), with heights of 24 nm ± 5 nm (measured using AFM). Electrodeposition carried out at the much lower driving force, +550 mV for 15 s (Figure 4(c)) produced larger Au NPs with heights ~ 43 nm ± 8 nm and considerably lower coverages; one order of magnitude lower, ~ 22 ± 3 NPs $µm^{-2}$. Furthermore, high resolution FE-SEM images (Figure 4(b,c) showed that the electrodeposited Au NPs were polycrystalline, with evidence of some faceting.

An effective surface coverage for the two different Au nanostructures was determined via analysis of the charge associated with a gold oxide stripping peak. In 0.1 M PBS (pH 7.2) an oxidation potential (+1.2 V) was applied to the electrode for 20 s to form the surface oxide. After this time period the current decreased to zero, indicating that the Au surface oxidation was complete. Figure 5 shows the stripping peaks obtained at the two different electrode types and an evaporated Au UME after cathodically sweeping the potential from +0.9 V to 0.1 V, at a scan rate of 20 mV s^{-1}, to remove the oxide formed. The stripping peak potential was +0.44 V for both Au NP-SWNT structures and +0.43 V for the Au_{evap} surface.

The charge associated with the stripping peak recorded on the Au_{evap} was found to be 320 µC cm^{-2} which is slightly smaller than the reported value[28] for a solid polished polycrystalline Au electrode. This is likely to be due to the reduced surface roughness of Au_{evap} compared to polished polycrystalline Au. Defining the surface coverage, θ, of Au_{evap} to be 100%, an effective surface coverage for the two Au NP-SWNT structures was determined from consideration of the charge passed during oxide stripping for these two electrodes. Au NPs deposited at +550 mV for 15 s gave θ ~ 35% whilst the Au NPs grown at –800 mV for 12 s resulted in θ ~ 92%. These effective θ values also qualitatively agree well with the magnitudes of the charge passed

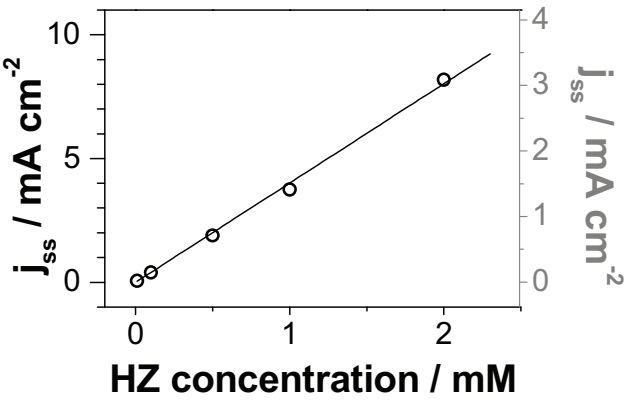

Figure 7. Steady state current density, j_{ss}, versus HZ concentration plot for Au NP-SWNT electrodes, derived using a surface coverage θ = 35 % (black scale) and θ = 92 % (gray scale).

during cycling of the three electrodes in 0.1 M PBS at 100 mV s^{-1} (Figure 5 inset).

Figure 6 shows the CV characteristics for 0.5 mM HZ oxidation in 0.1 M PBS recorded at 10 mV s^{-1} for the two Au NP-SWNT electrode structures shown in Figures 4(b,c) and a planar Au_{evap} UME of the same geometric dimension. Notably, the CV for HZ oxidation at the Au disc UME (red line) is significantly shifted by ca. 200 mV more positive ($E_{1/2}$ = 0.256 V) compared to both of the Au NP-SWNT electrodes. $E_{1/2}$ for HZ oxidation on Au polycrystalline electrodes has been observed at similar potentials to that seen herein for Au_{evap}.[21, 29]

This indicates that the HZ oxidation reaction is more facile on a SWNT surface containing the polycrystalline Au NPs than at a thin Au film electrode. As the flux of HZ to the individual Au NPs particles is higher than to the planar Au UME, based on the calculated θ values[30] (see above), the shift negative in $E_{1/2}$ for the Au NP-SWNT electrode (compared to planar Au) is not due to a difference in effective mass transport and is more likely to reflect the fact that the polycrystalline Au NPs presents a more active catalytic surface for HZ oxidation. In Figure 6 the onset of a cathodic current ca. −0.15 V over the Au NP electrode corresponds to O_2-reduction[7, 31] which again is more facile on the Au NP surfaces than Au_{evap}.

Focusing on the CV response of the two Au NP electrodes, the higher θ electrode has an $E_{1/2}$ ($E_{1/2}$ = 0.058 V ± 0.005 V) slightly less positive than for the lower θ electrode ($E_{1/2}$ = 0.082 V ± 0.006 V). This interesting experimental observation could result from the fact as the Au NP coverage increases, the flux to each particle decreases[30] and thus the demands placed on each NP, in terms of HZ turnover, is less resulting in a slightly less positive overpotential. A similar phenomenon was observed for the electro-oxidation of CO at citrate stabilized Au NPs on an indium tin oxide coated glass surface, where $E_{1/2}$ was found to shift more negative as the surface coverage (number density) increased (for a constant particle size).[32]

A diffusion-limited current of similar magnitude is evident in each of the CVs shown in Figure 6 and using equation 1 it is possible to determine n for the oxidation process assuming D_{HZ} = 1.4 × 10^{-5} cm s^{-1} [29]. n is thus calculated as 3.8 ($Au_{evap.}$), 3.9 (E_{dep} = +550 mV) and 3.7 (E_{dep} = -800 mV) for the three electrodes, each agreeing well with the literature value of 4.[21, 29] Furthermore, values for the diffusion-corrected Tafel slopes[33] for the electro-oxidation of HZ at the two Au NP - SWNT surfaces were determined as 93 ± 7 mV (low coverage) and 86 ± 3 mV (higher coverage) respectively. These values are similar to those reported for the oxidation of HZ at self assembled citrate stabilized Au NPs (70-100 nm)[34] on a polycrystalline gold electrode.[29] The observed difference in the Tafel slope values may indicate that different crystallographic orientations dominate in the two differently deposited Au NP structures.[21] For example, it has been observed previously using single crystal electrodes that the Au(100) surface provides more facile electron transfer characteristics for HZ oxidation than both the (110) and (111) surfaces.[21]

Steady-state CVs as a function of HZ concentration were also recorded in order to determine the limiting current density – concentration sensitivity of the electrode, (Figure 7). The gradient of the plot of steady-state current density, normalized by θ, versus HZ concentration gave sensitivity values of 1.5 mA cm^{-2} mM^{-1} for the highest surface coverage (θ = 92%) and 3.9 mA cm^{-2} mM^{-1} (θ = 35 %). While there may be room for improvement by reducing the Au NP surface coverage even further, it is important to point out that these values are higher than achieved with other metal nanoparticle CNT functionalized electrodes, such as Pt NP – multi-walled NTs (MWNTs),[35] Ag NPs supported on MWNTs[36] and other graphitic electrode surfaces e.g. Pd nanoislands on highly orientated pyrolytic graphite.[37]

Conclusions

SWNT network UMEs, grown via cCVD on an insulating substrate provide a very effective conductive support for the direct electrodeposition of electrocatalytically active Au NPs. Compared to SWNT growth procedures, the use of cCVD produces SWNTs which contain negligible amounts of electrocatalytically active metal impurity. For the electro-oxidation of HZ, the SWNT network electrode was found to be completely inactive towards HZ electro-oxidation probably because neither HZ nor the reactive intermediates adsorb effectively at the surface of a SWNT.

Electrocatalytic activity was bestowed on the network in a controlled and deliberate manner by electrodepositing Au NPs of a defined number density and size distribution. Two different structures were chosen for study; the first contained polycrystalline Au NPs at a number density of 250 NPs ± 13 μm^{-2} and heights 24 nm ± 5 nm and the second with polycrystalline Au NPs of height 43 nm ± 8 nm and density ~ 22 ± 3 NPs μm^{-2}. Effective surface coverages, θ, were determined for both from consideration of the charge passed during stripping of deliberately formed gold oxide from the surface; in particular θ = 92% (high coverage), θ = 35% (lower coverage). Both NP morphologies showed a significant cathodic potential shift by ca. 200 mV, for HZ oxidation, compared to a gold disc UME of the same geometric area, indicating significantly more facile electron transfer kinetics at the Au NP-SWNT electrodes.

The Au NP-SWNT structure with θ = 92% showed a further slight cathodic potential shift, by ca. 20 mV, for HZ oxidation compared to the θ = 35% Au NP electrode. This was attributed to the lower flux of reactant to individual NPs at the higher coverage surface. The limiting current density sensitivities per

unit HZ concentration for the Au NP – SWNT UMEs were found to be higher than for many other metal NP functionalized CNT electrodes.

Acknowledgements

We thank Dr. Aleix G. Güell for help with the Raman microscopy experiment and his valuable comments during the preparation of the manuscript. Helpful discussions and advice from Dr. Ioana Dumitrescu, Dr. Jonathan Edgeworth and Dr. Laura Hutton are also acknowledged. We thank EPSRC [EP/H023909/1] and the European Research Council ERC-2009-AdG 247143-QUANTIF (PRU and PVD) for support. Part of the equipment used in this research was obtained through Birmingham Science City with support from Advantage West Midlands and the European Regional Development Fund.

Notes and references

Chemistry Department, University of Warwick, Gibbet Hill Road Coventry, CV4 7AL, United Kingdom. Fax: +44 2476 524112; Tel: +44 2476 573886; E-mail: P.R.Unwin@warwick.ac.uk, J.Macpherson@warwick.ac.uk

1. D. Hernández-Santos, M. B. González-García and A. C. García, *Electroanalysis*, 2002, **14**, 1225-1235.
2. C. Welch and R. Compton, *Anal. Bioanal. Chem.*, 2006, **384**, 601-619.
3. P. Avouris, *Acc. Chem. Res.*, 2002, **35**, 1026-1034.
4. S. Rosenblatt, Y. Yaish, J. Park, J. Gore, V. Sazonova and P. L. McEuen, *Nano Lett.*, 2002, **2**, 869-872.
5. I. Dumitrescu, P. R. Unwin and J. V. Macpherson, *Chem. Commun.*, 2009, 6886-6901.
6. S. Hrapovic, E. Majid, Y. Liu, K. Male and J. H. T. Luong, *Anal. Chem.*, 2006, **78**, 5504-5512.
7. P. V. Dudin, P. R. Unwin and J. V. Macpherson, *J. Phys. Chem. C*, 2010, **114**, 13241-13248.
8. T. M. Day, P. R. Unwin and J. V. Macpherson, *Nano Lett.*, 2006, **7**, 51-57.
9. T. M. Day, P. R. Unwin, N. R. Wilson and J. V. Macpherson, *J. Am. Chem. Soc.*, 2005, **127**, 10639-10647.
10. B. M. Quinn, C. Dekker and S. G. Lemay, *J. Am. Chem. Soc.*, 2005, **127**, 6146-6147.
11. K. Jurkschat, X. Ji, A. Crossley, R. G. Compton and C. E. Banks, *Analyst*, 2007, **132**, 21-23.
12. M. Pumera and H. Iwai, *J. Phys. Chem. C*, 2009, **113**, 4401-4405.
13. J. Kruusma, N. Mould, K. Jurkschat, A. Crossley and C. E. Banks, *Electrochem. Commun.*, 2007, **9**, 2330-2333.
14. E. J. E. Stuart and M. Pumera, *J. Phys. Chem. C*, 2010, **114**, 21296-21298.
15. I. Dumitrescu, J. P. Edgeworth, P. R. Unwin and J. V. Macpherson, *Advanced Materials*, 2009, **21**, 3105-3109.
16. I. Dumitrescu, P. R. Unwin, N. R. Wilson and J. V. Macpherson, *Anal. Chem.*, 2008, **80**, 3598-3605
17. P. Bertoncello, J. P. Edgeworth, J. V. Macpherson and P. R. Unwin, *J. Am. Chem. Soc.*, 2007, **129**, 10982-10983.
18. A. Rutkowska, T. M. Bawazeer, J. V. Macpherson and P. R. Unwin, *Phys. Chem. Chem. Phys.*, 2011, **13**, 5223-5226.
19. G. Choudhary and H. Hansen, *Chemosphere*, 1998, **37**, 801-843.
20. G. E. Evans and K. V. Kordesch, *Science*, 1967, **158**, 1148-1152.
21. B. Alvarez-Ruiz, R. Gomez, J. M. Orts and J. M. Feliu, *J. Electrochem. Soc.*, 2002, **149**, D35-D45.
22. A. P. O'Mullane, S. E. Dale, T. M. Day, N. R. Wilson, J. V. Macpherson and P. R. Unwin, *J. Solid State Electrochem.*, 2006, **10**, 792-807.
23. C. Fantini, A. Jorio, M. Souza, M. S. Strano, M. S. Dresselhaus and M. A. Pimenta, *Phys. Rev. Lett.*, 2004, **93**, 147406.
24. X. Feng, S. Irle, H. Witek, K. Morokuma, R. Vidic and E. Borguet, *J. Am. Chem. Soc.*, 2005, **127**, 10533-10538.
25. I. Dumitrescu, P. V. Dudin, J. P. Edgeworth, J. V. Macpherson and P. R. Unwin, *J. Phys. Chem. C*, 2010, **114**, 2633-2639.
26. A. J. Bard, and Faulkner, L. R., *Electrochemical Methods: Fundamentals and Applications*, Wiley, New York, 2000.
27. J. L. Conyers and H. S. White, *Anal. Chem.*, 2000, **72**, 4441-4446.
28. D. Dickertmann, J. W. Schultze and K. J. Vetter, *J. Electroanal. Chem. Interfac.*, 1974, **55**, 429-443.
29. U. Eisner and Y. Zemer, *J. Electroanal. Chem.*, 1972, **38**, 381-388.
30. C. Amatore, J. M. Savéant and D. Tessier, *J. Electroanal. Chem. Interfac.*, 1983, **147**, 39-51.
31. M. S. El-Deab, T. Sotomura and T. Ohsaka, *J. Electrochem. Soc.*, 2005, **152**, C730-C737.
32. S. Kumar and S. Zou, *J. Phys. Chem. B*, 2005, **109**, 15707-15713.
33. I. Streeter and R. G. Compton, *Electrochim. Acta*, 2007, **52**, 4305-4311.
34. B. K. Jena and C. R. Raj, *J. Phys. Chem. C*, 2007, **111**, 6228-6232.
35. S. Chakraborty and C. R. Raj, *Sensors and Actuators B: Chemical*, 2010, **147**, 222-227.
36. G. Gao, D. Guo, C. Wang and H. Li, *Electrochem. Commun.*, 2007, **9**, 1582-1586.
37. Y. Gimeno, A. Hernández Creus, S. González, R. C. Salvarezza and A. J. Arvia, *Chem. Mater.*, 2001, **13**, 1857-1864.

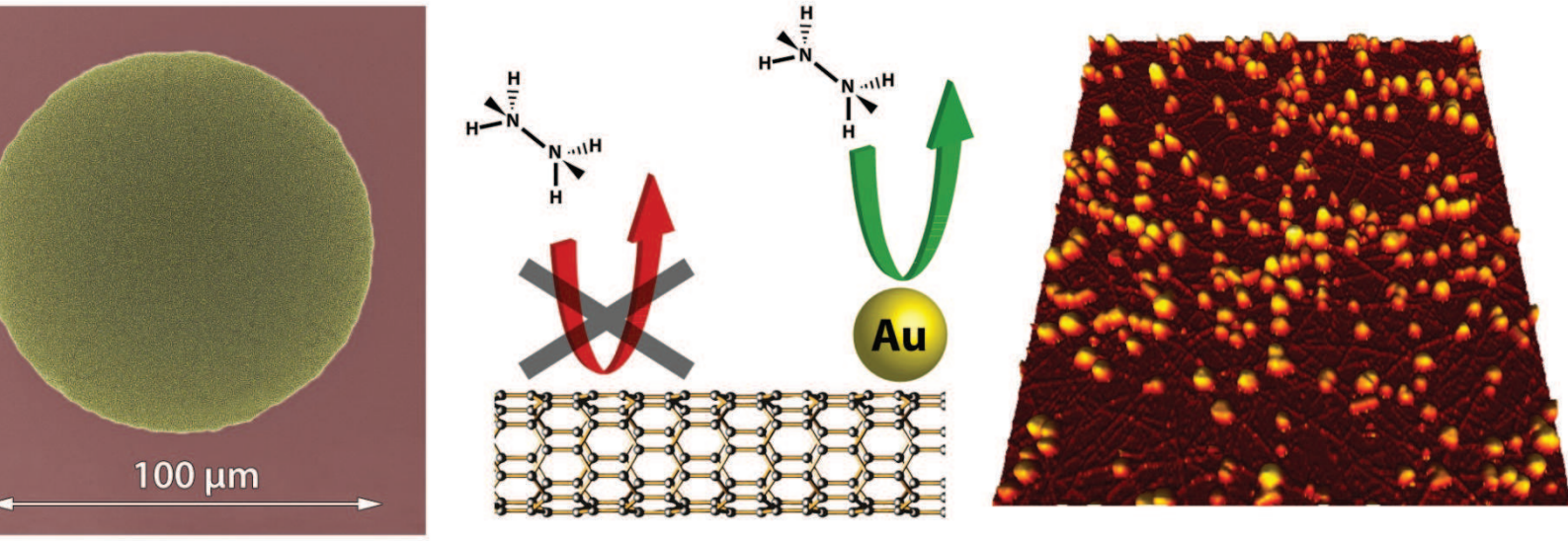

controlled addition of Au metal nanoparticles to single walled nanotube network
amicroelectrodes results in highly sensitive electrodes for the detection of hydrazi

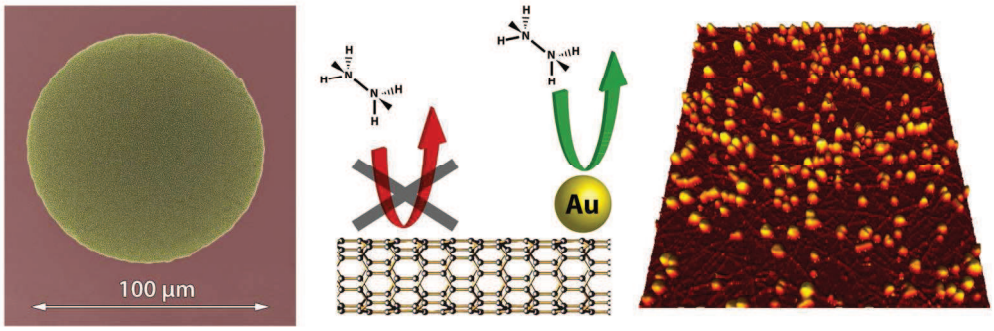

TOC jpg file
169x59mm (300 x 300 DPI)